Biochimica et Biophysica Acta 1787 (2009) 584–592

Contents lists available at ScienceDirect

Biochimica et Biophysica Acta

journal homepage: www.elsevier.com/locate/bbabio

Review

New pulsed EPR methods and their application to characterize mitochondrial complex I

Thorsten Maly [a], Klaus Zwicker [b], Adrian Cernescu [c], Ulrich Brandt [b], Thomas F. Prisner [c,*]

[a] Francis Bitter Magnet Laboratory and Department of Chemistry, Massachusetts Institute of Technology, Cambridge, MA 02139, USA
[b] Molecular Bioenergetics Group, Cluster of Excellence Frankfurt "Macromolecular Complexes", Medical School, Johann Wolfgang Goethe-Universität, Frankfurt am Main, Germany
[c] Institut für Physikalische und Theoretische Chemie, Johann Wolfgang Goethe-Universität Frankfurt, D-60439 Frankfurt am Main, Germany

ARTICLE INFO

Article history:
Received 12 December 2008
Received in revised form 4 February 2009
Accepted 5 February 2009
Available online 12 February 2009

Keywords:
Complex I
Iron–sulfur cluster
Pulsed EPR
REFINE
Hyperfine spectroscopy

ABSTRACT

Electron Paramagnetic Resonance (EPR) spectroscopy is the method of choice to study paramagnetic cofactors that often play an important role as active centers in electron transfer processes in biological systems. However, in many cases more than one paramagnetic species is contributing to the observed EPR spectrum, making the analysis of individual contributions difficult and in some cases impossible. With time-domain techniques it is possible to exploit differences in the relaxation behavior of different paramagnetic species to distinguish between them and separate their individual spectral contribution. Here we give an overview of the use of pulsed EPR spectroscopy to study the iron–sulfur clusters of NADH:ubiquinone oxidoreductase (complex I). While FeS cluster N1 can be studied individually at a temperature of 30 K, this is not possible for FeS cluster N2 due to its severe spectral overlap with cluster N1. In this case Relaxation Filtered Hyperfine (REFINE) spectroscopy can be used to separate the overlapping spectra based on differences in their relaxation behavior.

1. Introduction

Paramagnetic molecules, such as organic radicals or metal centers play an important role in biological systems and are in many cases the active centers for electron transfer reactions [1–4]. To study these cofactors, the method of choice is Electron Paramagnetic Resonance (EPR) spectroscopy and the most widely employed technique uses continuous wave (cw) microwave irradiation at a frequency of 9 GHz. In recent years pulsed EPR methods (e.g. ESEEM, HYSCORE, PELDOR) have extended the standard repertoire of EPR techniques and today such hyperfine and dipolar methods can be used to characterize the paramagnetic center itself, its ligand sphere as well as interactions with other EPR active centers up to 8 nm away [5–7].

Unlike NMR spectroscopy, EPR often has single-site resolution since the number of paramagnetic species is limited in the sample. However, a common problem especially in studying biological systems is the presence of more than one paramagnetic species contributing to the overall observed EPR spectrum. This usually results in severe overlap of spectral features from different paramagnetic species, making the analysis of individual contributions difficult and in some cases impossible.

If the paramagnetic species have different g-values, one possibility to separate overlapping spectra is to perform EPR experiments at high magnetic field strengths. Also Electron Nuclear Double Resonance (ENDOR) experiments performed at high magnetic fields (>95 GHz) can dramatically improve and simplify hyperfine spectra [3,8,9]. Unfortunately this advantage does not hold for methods like Electron Spin Echo Envelope Modulation (ESEEM) or Hyperfine Sublevel Correlation (HYSCORE) spectroscopy, since these experiments rely on forbidden transitions, whose transition moments are considerably attenuated at high magnetic fields [10]. In addition, for many metal-based paramagnetic centers, such as iron–sulfur (FeS) centers or hemes, high-field EPR will not be able to separate different signals because of their large g tensor anisotropy.

In most cases, EPR experiments need to be performed at low temperatures due to their fast electron spin relaxation times. However, different paramagnetic species, such as organic radicals and metal-centers or clusters, may exhibit usually large differences in their characteristic relaxation times, especially at low temperatures [11]. Therefore time-domain techniques that exploit differences in the spin-lattice relaxation time (T_1) or the phase memory time (T_2) will allow distinguishing them. Already the most commonly used two-pulse Hahn-echo or three-pulse stimulated echo sequence provides

Abbreviations: BDPA, α,γ-Bisdiphenylene-β-phenylallyl; BDPA/PS, BDPA dissolved in polystyrene; Complex I, NADH:ubiquinone oxidoreductase; CuHis, Copper Histidine Complex; DOSY, Diffusion Ordered Spectroscopy; ENDOR, Electron Nuclear Double Resonance; EPR, Electron Paramagnetic Resonance; ESEEM, Electron Spin Echo Envelope Modulation; FeS, Iron–sulfur; HYSCORE, Hyperfine Sublevel Correlation; iLT, inverse Laplace transformation; NADH, Nicotineamide Adenine Dinucleotide; NMR, Nuclear Magnetic Resonance; PELDOR, Pulsed Electron Double Resonance; REFINE, Relaxation Filtered Hyperfine; ROS, Reactive Oxygen Species; TEMPO, 2,2,6,6-Tetramethylpiperidine-1-oxyl; TEMPO/PS, TEMPO dissolved in polystyrene

* Corresponding author: Fax: +49 69 798 29406.
E-mail address: prisner@chemie.uni-frankfurt.de (T.F. Prisner).

0005-2728/$ – see front matter © 2009 Elsevier B.V. All rights reserved.
doi:10.1016/j.bbabio.2009.02.003

filter capabilities to separate EPR spectra by their T_2 or T_1 relaxation times [12,13].

This article covers recent developments of pulsed EPR methodology to separate overlapping spectra on the basis of their different relaxation behavior. The focus will be on experiments performed on model compounds to demonstrate the general applicability of such relaxation filters, and first applications to the FeS clusters in complex I of mitochondrial respiration will be shown.

2. Iron–sulfur clusters in complex I

Mitochondrial NADH:ubiquinone oxidoreductase (complex I), the first complex of the respiratory chain, is among the largest and most complicated membrane-bound protein complexes known [14,15]. It links the electron transfer from NADH to ubiquinone with the concomitant translocation of four protons across the inner membrane [16,17]. Because of its central role in respiration, mutations in complex I can lead to a large number of human disorders [18,19]. Furthermore, complex I has been suggested to be a major source of Reactive Oxygen Species (ROS) in mitochondria [20].

The protein complex from mammalian mitochondria is composed of 45 different subunits with a total molecular mass of nearly 1000 kDa [21], but smaller versions can be found in many bacteria [22]. In the obligate aerobic yeast *Yarrowia lipolytica*, a powerful model system for the structural and functional analysis of complex I [23,24], this enzyme also comprises at least 40 different subunits [25]. Complex I has a typical L-shaped structure, in which the hydrophobic arm is embedded in the membrane and the hydrophilic peripheral part protrudes into the mitochondrial matrix or the bacterial cytoplasm [26–29]. Cw EPR studies have revealed the presence of several paramagnetic cofactors such as iron–sulfur (FeS) clusters and quinones [30–34]. Depending on the organism, complex I hosts up to nine FeS centers [35,36] but not all of them are detectable by EPR because of a diamagnetic oxidation state or electron spin relaxation that is too fast. EPR spectra of *Y. lipolytica* are similar to those of complex I from bovine heart and *Neurospora crassa* [24,30]. In its NADH reduced state, the EPR spectra of five FeS clusters are detectable, designated N1 to N5. Cluster N1 is the only EPR detectable binuclear FeS center in complex I, while clusters N2–N5 are tetranuclear FeS clusters [23].

In Fig. 1 the temperature dependence of 9 GHz (X-band) field-sweep spectra of complex I from *Y. lipolytica* are shown. At 30 K only cluster N1 contributes to the echo-detected EPR spectrum. When lowering the temperature, more and more FeS clusters become visible. At 17 K cluster N1 and N2 contribute equally to the spectrum, while at a temperature of 5 K all five FeS clusters, with their own characteristic *g* tenor, are detectable [23].

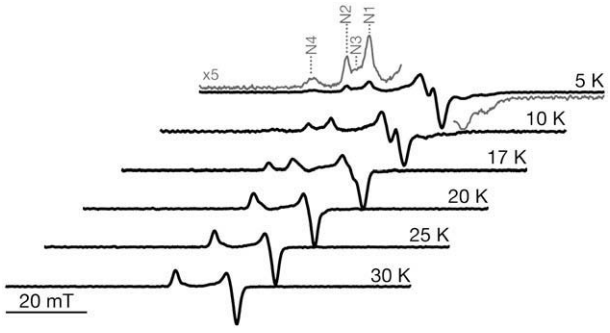

Fig. 1. Temperature dependence of the 9 GHz EPR spectra of complex I from *Y. lipolytica*. Pseudomodulated spectra (1 mT) of the echo-detected absorption spectra are shown and principal g_{zz} tensor components for clusters N1 to N4 are indicated. Figure adapted from [41]. The *g* tensor values are (g_{xx}, g_{yy}, g_{zz}): N1 (2.018, 1.945, 1.933), N2 (2.051, 1.926, 1.918), N3 (2.031, 1.930, 1.861), N4 (2.104, 1.931, 1.892) and N5 (2.062, 1.93, ~1.89), taken from [23].

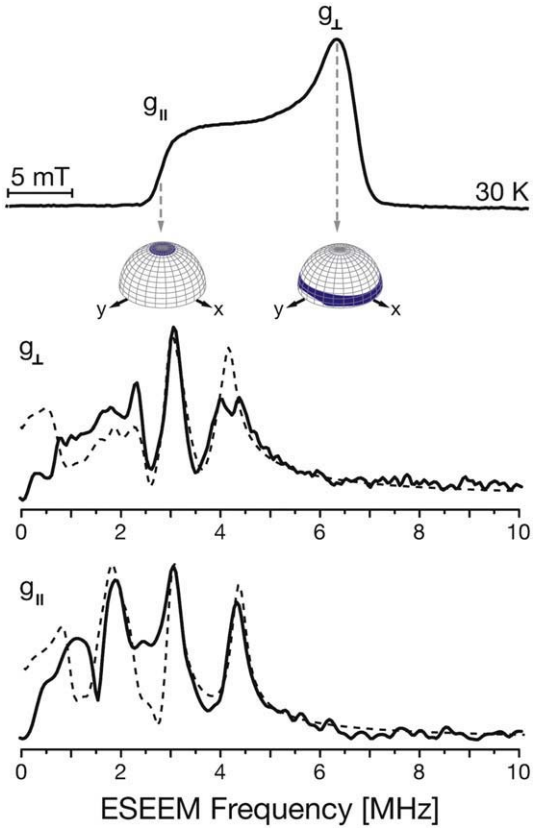

Fig. 2. (Top) 9 GHz field-sweep spectrum of complex I from *Y. lipolytica* at 30 K. The principal *g* tensor components $g_{||}$ and $g_{\perp}$ of cluster N1 are indicated and the respective orientation selection is shown below. (Middle and bottom) Three-pulse ESEEM spectra, taken at field positions corresponding to $g_{||}$ and $g_{\perp}$. Simulations are shown as dashed lines (parameter given in text). Figure taken from [41].

3. Characterization of cluster N1 by hyperfine spectroscopy

At 30 K only cluster N1 contributes to the echo-detected field-sweep spectrum and can therefore be studied individually. The field-swept echo-detected powder spectrum is characterized by the components of the axial symmetric *g* tensor $g_{\perp}$ and $g_{||}$ (Fig. 2, top). The structural information content of such a field-sweep spectrum is nevertheless very limited because hyperfine interactions of the paramagnetic center with nuclei in its close proximity and dipolar interactions to other FeS clusters are hidden by the large inhomogeneous linewidth. On the other hand this large *g* anisotropy provides the possibility to record single-crystal like EPR spectra, since for a given magnetic field position and a microwave excitation bandwidth much smaller than the overall EPR linewidth, only a subset of molecular orientations is excited [37]. This is shown in Fig. 2, where the orientations of the magnetic field in the molecular axis system of N1, which contribute to the EPR signal, are indicated on a sphere for two different values of the magnetic field. Therefore hyperfine techniques such as ESEEM and HYSCORE can be used to study such interactions and can reveal much information about the local surrounding of the paramagnetic center [38–41].

In Fig. 2 (bottom), 9 GHz three-pulse ESEEM spectra, recorded at magnetic field positions corresponding to the principal *g* tensor values $g_{\perp}$ and $g_{||}$ of cluster N1, are shown. These features can be assigned to a hyperfine interaction of the FeS cluster with a nitrogen nucleus in close proximity, and arise from single-quantum (sq) and

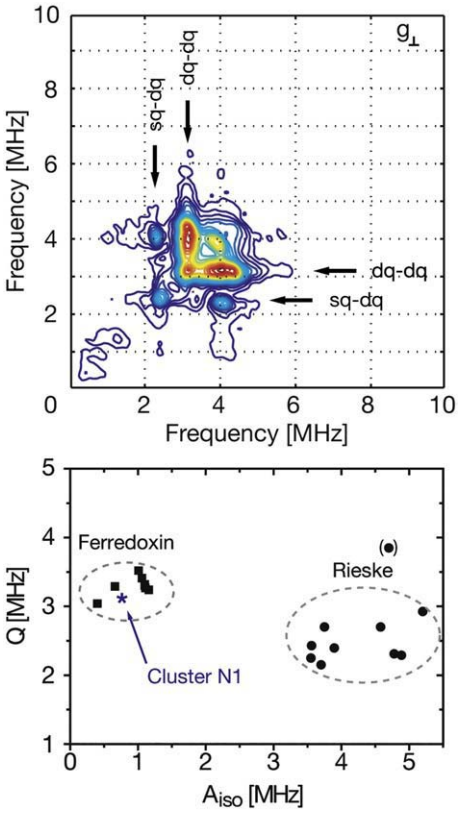

Fig. 3. (Top) 9 GHz ^{14}N-HYSCORE spectrum ((+,+)-quadrant) of cluster N1 taken at a field position corresponding to $g_\perp$, $T=30$ K. The arrows indicate the ^{14}N dq–dq and sq–dq correlation peaks. (Bottom) Hyperfine and quadrupole parameters of different [2Fe–2S] clusters of metalloproteins including cluster N1 of *Y. lipolytica*. The circles indicate two different types of coordination referred to as Rieske-type and ferredoxin-type. The hyperfine and quadrupole coupling constants determined of a ^{14}N nucleus interacting with cluster N1 are indicated by the asterisk. Figures taken from [41].

double-quantum (dq) transitions within the ^{14}N ($I=1$) nuclear manifolds. To simplify the analysis of the observed ESEEM spectra, two-dimensional HYSCORE experiments at X-band frequencies have been performed. In such an experiment, correlation peaks between nuclear transitions of the different electronic spin states $m_S=\pm 1/2$ can be observed. In Fig. 3 (top), a HYSCORE spectrum of cluster N1, taken at a magnetic field position corresponding to $g_\perp$ is shown. The observed correlation peaks can be assigned to dq–dq and sq–dq transitions of the ^{14}N nucleus. The analysis of the HYSCORE spectrum allows the conclusion that only a single ^{14}N nucleus couples to the electron spin of cluster N1. From numerical simulations of the ESEEM spectra following the procedure developed by Kevan and Bowman [42] an isotropic hyperfine coupling constant of 0.9 MHz, a quadrupole coupling constant of 3.1 MHz and an asymmetry parameter $\eta=0.5$ was obtained. By comparing these values with coupling parameters of ^{14}N nuclei interacting with FeS cluster obtained for different organisms, cluster N1 can be clearly identified as a FeS cluster in a ferrodoxin-type coordination [41]. This result was later confirmed in the X-ray crystal structure of the peripheral arm of bacterial complex I [36].

Besides the hyperfine interaction to a nitrogen nucleus, more features are observed in the 9 GHz HYSCORE spectrum of cluster N1 in the region between 10 and 20 MHz (Fig. 4). Two large ridges are observed in the HYSCORE spectrum (Fig. 4, left), centered at a frequency of ~15 MHz, which identifies them as hyperfine interactions between the FeS cluster and surrounding protons. To analyze the observed ridges, the HYSCORE spectrum can be represented in a coordinate system in which the axes are squared. The isotropic as well as the anisotropic values for the hyperfine interaction can easily be determined from this representation [43]. Such an analysis for the proton region is shown in Fig. 4 (right): two protons interacting with the FeS center can be identified having anisotropic couplings of 6.0 and 3.5 MHz and isotropic couplings of 2.4 (−8.4) and 1.4 (−4.9) MHz, respectively [41]. Because the sign of the hyperfine coupling cannot be obtained by this method, two values for the isotropic coupling are possible (values given in parenthesis). Similar values for the hyperfine coupling are obtained from a correlation-peak experiment (Fig. 4, middle panel). In this four-pulse ESEEM experiment the evolution time τ is varied while evolution times t_1 and t_2 are varied simultaneously (see Fig. 5 and [44] for details). After Fourier transformation, this experiment yields the projection of the HYSCORE spectrum onto the diagonal $\omega_2=\omega_1$ and combination peaks appear as narrow features in the spectrum since the orientation-dependent hyperfine interactions are partially refocused [44]. The observed hyperfine couplings are in the typical range for β-protons of cysteins ligating FeS clusters [45,46].

4. Separation of two spectrally overlapping species

At a temperature of 17 K the 9 GHz EPR spectrum of complex I from *Y. lipolytica* shows contributions from both clusters, N1 and N2 (Fig. 1). In this case, special spectral editing techniques have to be used, to study both clusters individually by EPR spectroscopy. Here, an inversion-recovery filter (IRf) allowed the separation of N1 and N2 by their differences in the T_1 relaxation times.

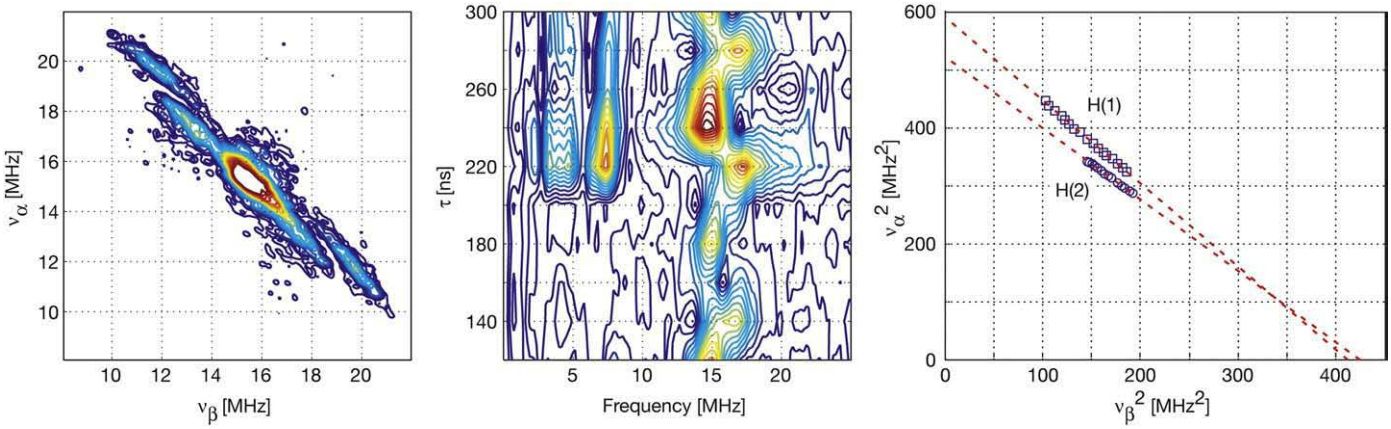

Fig. 4. (Left) 9 GHz ^{1}H-HYSCORE spectrum ((+,+)-quadrant) of cluster N1 taken at a field position corresponding to $g_\perp$, $T=30$ K. (Middle) Combination peak experiment taken at the same magnetic field position. (Right) Selected points on the ridge of the ^{1}H-HYSCORE (shown to the left). The data points are presented in a squared-axes representation for a graphical determination of the hyperfine coupling parameters (for more information see text). Figure adapted from [41].

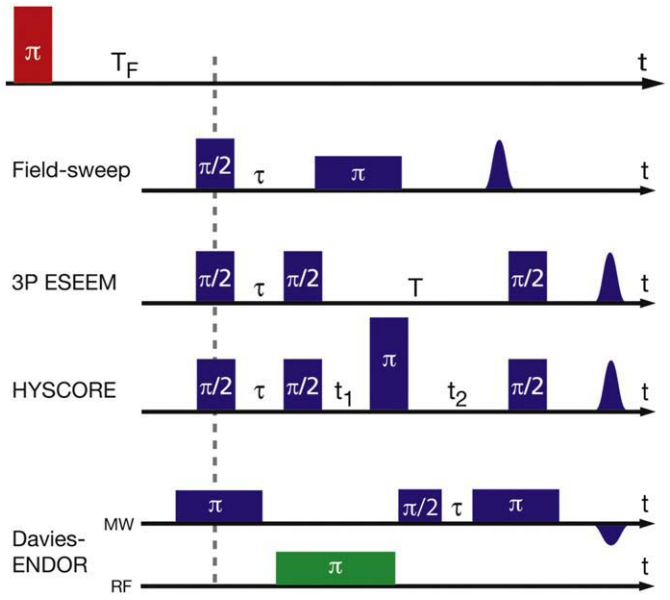

Fig. 5. Pulse sequences for relaxation filtered experiments. The inversion-recovery filter consists of an inversion pulse followed by a delay T_F. The filter sequence is followed by commonly used EPR pulse sequences such as echo-detected field sweep, three-pulse ESEEM, HYSCORE or Davies-ENDOR.

The pulse sequence for an inversion-recovery experiment is given in Fig. 5. After the initial π inversion-pulse the non-Boltzmann polarization of the electron spin will relax back to its thermal equilibrium magnetization with its characteristic longitudinal relaxation time T_1. During this process the macroscopic magnetization traverses a zero-crossing point (Fig. 6, top). In a mixture of two species, with different relaxation times T_1^s (slow) and T_1^f (fast), each species will traverse its own zero-crossing point at a filter time of T_F^s or T_F^f, as indicated in Fig. 6 by the arrows. Therefore, only the EPR spectrum of the fast or slow relaxing species is detected if the field-sweep spectrum is recorded with the filter time T_F set to either T_F^f or T_F^s. This technique shows the EPR spectra of the individual compounds when applied to a mixture of two species. However, in a more complex mixture of several paramagnetic species, this technique can still be useful to simplify crowded spectra by suppressing one species.

The efficiency of such a filter has been tested using a mixture of two model compounds BDPA/PS (slow) and TEMPO/PS (fast) in polystyrene (Fig. 6). The 9 GHz EPR spectrum of the mixture is shown in Fig. 6 (top, black). Using a filter time of $T_F^{BDPA} = 9$ μs or $T_F^{TEMPO} = 192$ ns the individual spectrum of TEMPO/PS or BDPA/PS is observed. For the species with the longer relaxation time (BDPA/PS), the inverted signal is obtained, with a signal intensity of 35% of the maximum intensity. Because of the much shorter relaxation time of TEMPO/PS almost 100% of the maximum signal intensity is observed for the fast relaxing species. A comparison of spectra obtained from the mixture with spectra of the pure compounds, shows an excellent agreement.

The inversion-recovery filter can be combined with every pulse EPR sequence for hyperfine spectroscopy such as ESEEM, HYSCORE or ENDOR. This technique is called Relaxation Filtered Hyperfine (REFINE) spectroscopy and some examples of pulse sequences are shown in Fig. 5. In general, the first pulse of the original pulse sequence is applied after the filter time T_F. Short filter times can create unwanted echoes that interfere with the measurements (13 for three-pulse REFINE-ESEEM), but they can be removed using an appropriate phase cycle [47].

In complex I, two nitrogen-containing amino acid residues had been suggested as possible candidates for the fourth ligand of iron–sulfur cluster N2 [48,49]. To test this hypothesis, cluster N2 was studied by X-band ESEEM spectroscopy, a difficult task due to the severe spectral overlap with cluster N1. Furthermore, the linewidths in an ESEEM experiment are very sensitive to temperature; therefore, observed differences in the 9 GHz ESEEM spectra taken at 30 and 17 K could easily be misinterpreted. To overcome this problem, IRf field-sweep and REFINE-ESEEM experiments were performed. In Fig. 7 (top panel) IRf field-sweep spectra of complex I taken at 17 K are shown. Using filter times of $T_F = 68$ ns and 420 ns allowed recording of spectra of cluster N1 and N2 separately. The same filter times can then be used in a REFINE-ESEEM experiment to study the hyperfine interactions of each FeS cluster individually. Such ESEEM time traces and their respective Fourier transformations are shown in Fig. 7 (middle and bottom panel). For comparison, an ESEEM experiment was also performed, using a filter time of $T_F = 50$ μs, at which the system is back at the thermal equilibrium polarization. Since the ESEEM spectra at $T_F = 50$ μs and $T_F = 68$ ns are similar, it can be concluded that only cluster N1 shows a hyperfine interaction with a ^{14}N nucleus and that cluster N2 is not ligated by a nitrogen-containing amino acid residue [50]. This was also seen later in the crystal structure of the hydrophilic domain of complex I that revealed a four-cysteine ligation of this cluster [36].

REFINE spectroscopy can also be applied to two-dimensional hyperfine methods, such as HYSCORE. In Fig. 8 the application of REFINE-HYSCORE to a mixture of a copper-histidine complex (CuHis) and BDPA in polystyrene (BDPA/PS) at a microwave frequency of 9 GHz is shown. Without a filter sequence, several correlation peaks

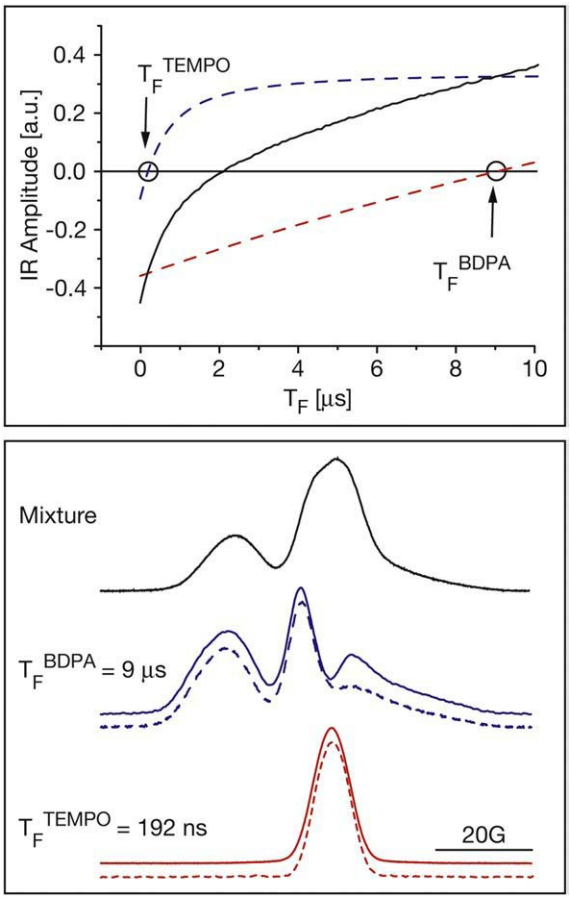

Fig. 6. (Top) 9 GHz Inversion-recovery traces of a mixture (black) of BDPA/PS (red) and TEMPO/PS (blue) as well as for the individual compounds taken at room temperature. The arrows indicate the zero-crossing points at T_F(TEMPO/PS) = 192 ns and T_F(BDPA/PS) = 9 μs. (Bottom) Field-sweep and IRf field-sweep spectra of the mixture as indicated. IRf field-sweep spectra are recorded with filter times obtained from inversion-recovery traces shown above. The spectra of the pure compounds (dashed lines) are compared to the spectra obtained from the mixture. Figures adapted from [50].

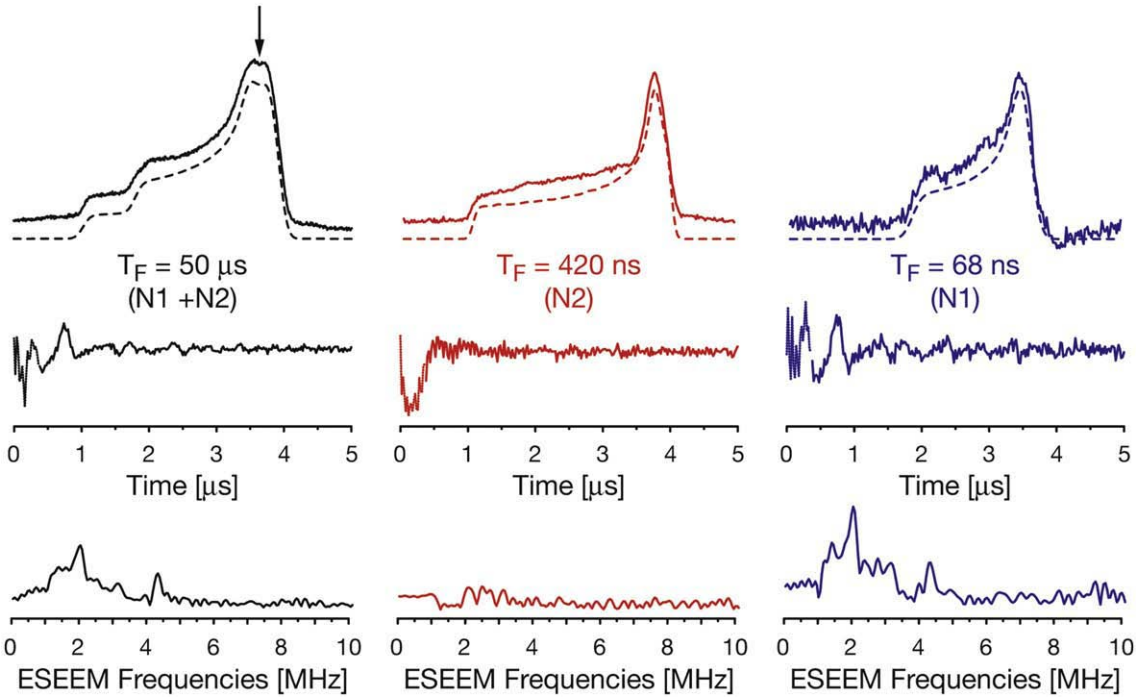

Fig. 7. (Top panel) 9 GHz Inversion-recovery filtered echo-detected field-sweep EPR spectra of complex I of *Y. lipolytica* at 17 K taken with filter times as indicated (simulations shown as dashed lines). Left: $T_F = 50$ µs (no filter effect), (Middle) $T_F = 420$ ns to select cluster N2 selectively. (Right) $T_F = 68$ ns to select cluster N1 selectively. (Middle panel) 9 GHz REFINE-ESEEM (three-pulse) time traces recorded with filter times as indicated. Spectra are recorded at a field position as indicated by the arrow (upper left spectrum). (Bottom panel) Fourier transform of the REFINE-ESEEM time traces shown above. Figure taken from [50].

are observed in the ^{14}N-region (CuHis) and the ^{1}H (BDPA) region of the HYSCORE spectrum (Fig. 8,A). Using the correct filter times to suppress either contributions of CuHis ($T_F^{CuHis} = 10$ µs) or BDPA/PS ($T_F^{BDPA/PS} = 850$ µs), it is possible to record a HYSCORE spectrum where only the ^{1}H correlation peaks of BDPA/PS (Fig. 8,B) or the ^{14}N correlation peaks of the CuHis complex (Fig. 8,C) are visible. The

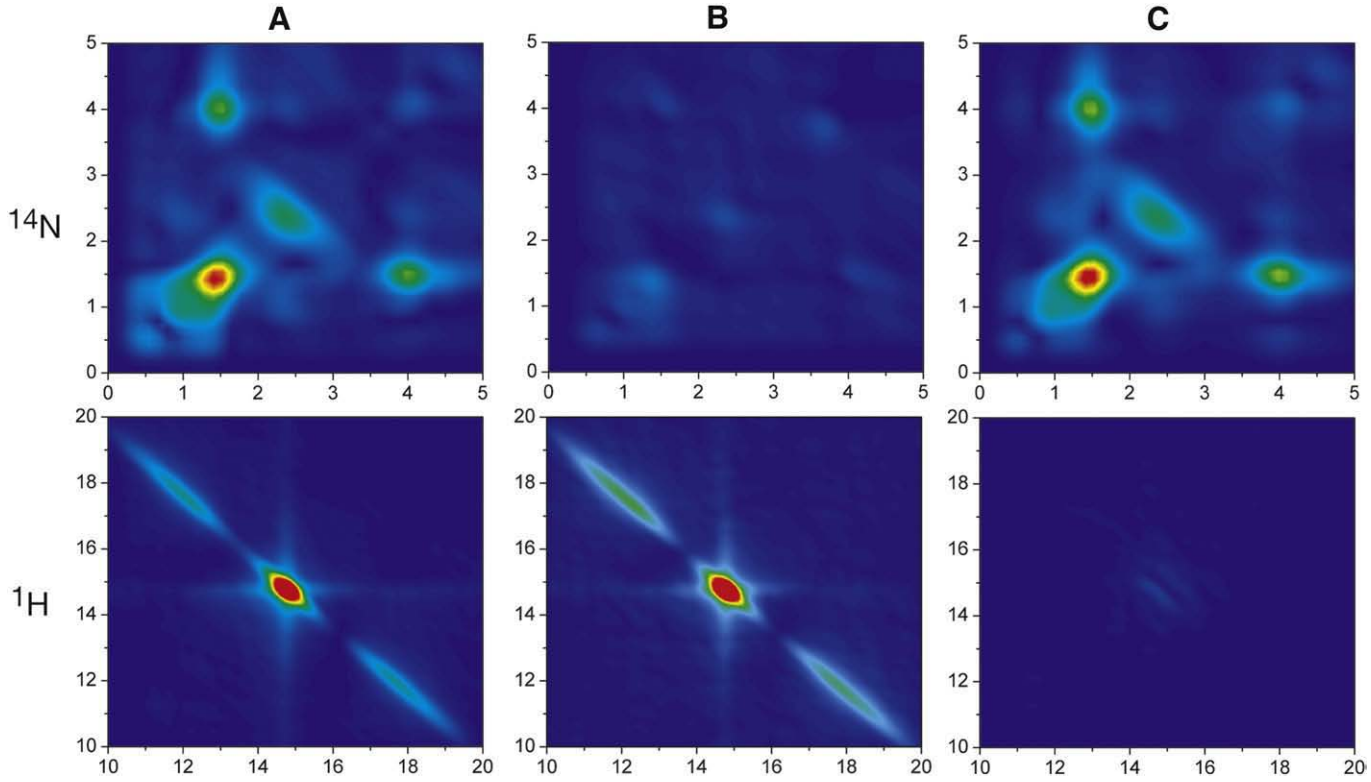

Fig. 8. 49 GHz ^{14}N and ^{1}H REFINE-HYSCORE spectra recorded from a mixture of a CuHis and BDPA, $T = 20$ K. Upper row: ^{14}N-region (0–5 MHz), lower row, ^{1}H-region (10–20 MHz). All surface plots are shown at the same contour level. (A) HYSCORE without filter sequence. (B) REFINE-HYSCORE with $T_F = 10$ µs. (C) REFINE-HYSCORE with $T_F = 850$ µs. All spectra are taken at a field position corresponding to $g = 2$. Figure taken from [61].

suppression of the ^{14}N contributions at a filter time of $T_F^{CuHis} = 10$ μs is about 95%, while at a filter time of $T_F^{BDPA/PS} = 850$ μs the suppression of ^1H contributions is almost 100%.

In a recent application of X-band REFINE-HYSCORE to biological systems, the method was used to study the nickel center of the active site of methyl-coenzyme M reductase (MCR) and to characterize the coordination sphere of two reduced paramagnetic states individually [51]. In another example, REFINE was used to study the cobalt bound to myoglobin. Here, two species had to be separated and the coordination spheres of each cobalt were studied by Q-band (35 GHz) REFINE-ENDOR [52]. This example demonstrates that even if the relaxation process shows a large anisotropy across the EPR line, a complete separation is possible (Fig. 19 in [52], supporting information).

5. Separation of several spectrally overlapping species

Using the concept of REFINE, it is possible to separate more than two spectrally overlapping species [53]. For this, the experiment has to be extended into a further dimension, which encodes the relaxation behavior of the individual species either by T_1 or T_2. If the paramagnetic species show a difference in their relaxation behavior, an inverse Laplace transformation (iLT) along this dimension leads to a separation of the different contributions. Since the numerical iLT is an ill-conditioned problem [54], a robust fitting algorithm, similar to those used in DOSY spectroscopy [55] can be used to perform the task [53,56].

The concept of two-dimensional REFINE is illustrated using the example of a REFINE-ESEEM experiment. The data set obtained in this experiment can be described by the following integral

$$S(\tau, T) = \int\int I(\nu, R) \cdot e^{i\nu 2\tau} \cdot G(R, T) \mathrm{d}\nu \mathrm{d}R, \quad (1)$$

with $S(\tau,T)$ the two-dimensional experimental data set, τ the evolution time of the ESEEM experiment, T the separation time in the relaxation domain, R the relaxation rates and $I(\nu,R)$ the desired REFINE-ESEEM spectrum with I the intensities of the ESEEM spectrum obtained after Fourier transformation and ν the ESEEM frequencies. $G(R,T)$ is called the relaxation kernel, a function that describes the relaxation process. For example for a saturation recovery experiment $G(R,T)$ is of the simple form $G(R,T) = 1 - e^{-T \cdot R}$. In the example described above, the desired REFINE-ESEEM spectrum $I(\nu,R)$ is obtained from $S(\tau,T)$ through inverting Eq. (1) by the following procedure:

$$S(\tau, T) \xrightarrow{iFT(\tau)} P(\nu, T) \xrightarrow{iLT(T)} I(\nu, R). \quad (2)$$

Here, prior to the inverse Laplace transformation, an inverse Fourier transformation has to be performed along the spectral dimension of the data set, including standard procedures such as appodization, linear prediction and zero-filling [57]. The result is a two-dimensional spectrum in which the spectral amplitudes are projected along the relaxation rate of the individual species. In the case of EPR or ENDOR spectra, that do not require a Fourier transformation, only the inverse Laplace transformation has to be performed.

The performance of two-dimensional REFINE spectroscopy is demonstrated on a simulated data set of five different species. Without any loss of generality, a field-sweep spectrum is chosen for the spectral domain while the relaxation domain is encoded by an inversion-recovery sequence. The five different species have (arbitrarily chosen) relaxation times of $T_1 = 1$, 4, 16, 64, and 256 μs and g values similar to the five iron–sulfur clusters observed in complex I (see caption of Fig. 1) [23]. Furthermore, for a realistic analysis 1% random noise was added to the simulated data set. The result of the analysis is shown in Fig. 9. After inverting the data set, five different species can be clearly identified (Fig. 9, left). The individual EPR spectrum of each species is obtained after projecting the signal amplitudes of each separated species along the mean value of the respective filter rate (Fig. 9, right). By varying factors such as number of species, signal amplitudes or amount of noise added, the following requirements for a successful separation were deduced:

1. *Signal-to-Noise ratio*: For mixtures of up to five different species the S/N ratio in the experimental two-dimensional REFINE data set has to be ≥100.
2. *Ratio of relaxation times*: In the presence of only two species the ratio can be as small as $T_1^A/T_1^B = 1{:}2$. If more species have to be separated, a ratio of 3–4 is sufficient. If different kinds of paramagnetic species are present (organic radicals, metal centers), this requirement is usually easily fulfilled.
3. *Number of species*: For S/N>100 and a ratio of relaxation times of >3, up to five species can be resolved easily.

It should be pointed out, that even with a large field dependence of the relaxation rates, caused, for example, by anisotropic librations [58], a separation is still possible, by following the contour lines in the individual field-sweep spectra.

In Fig. 10, an example of two-dimensional REFINE spectroscopy performed at X-band frequencies is shown. Here, the field-sweep spectra as well as the ESEEM spectra of a mixture of three spectrally overlapping components (CuHis, BDPA/PS and TEMPO/PS), which served as model system, are separated based on their different relaxation behavior.

Fig. 10 (top, left) shows a two-dimensional saturation-recovery detected field sweep spectrum. After inversion of the experimental data set, three signals with relaxation rates of 0.37, 1.2 and 2.08 kHz can be distinguished. Even for these rather similar relaxation rates, it was clearly possible to separate all three compounds from each other in the relaxation rate dimension. The individual components are

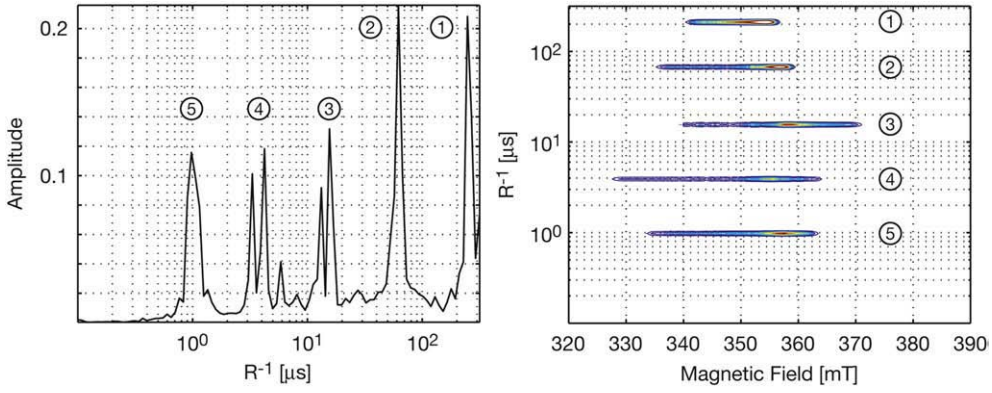

Fig. 9. Performance test of 2D REFINE to separate five different species. Right: Projection of the obtained relaxation filtered spectra along the magnetic field axis. Left: Contour plot of the 2D REFINE spectrum. Simulation parameters: Complex I g tensor values given in caption of Fig. 1. $T_1 = 1$, 4, 16, 64, 256 μs (N1, N2, N3, N4, N5). The resolution of the field axis is 700 pts and 100 filter times were used for the analysis.

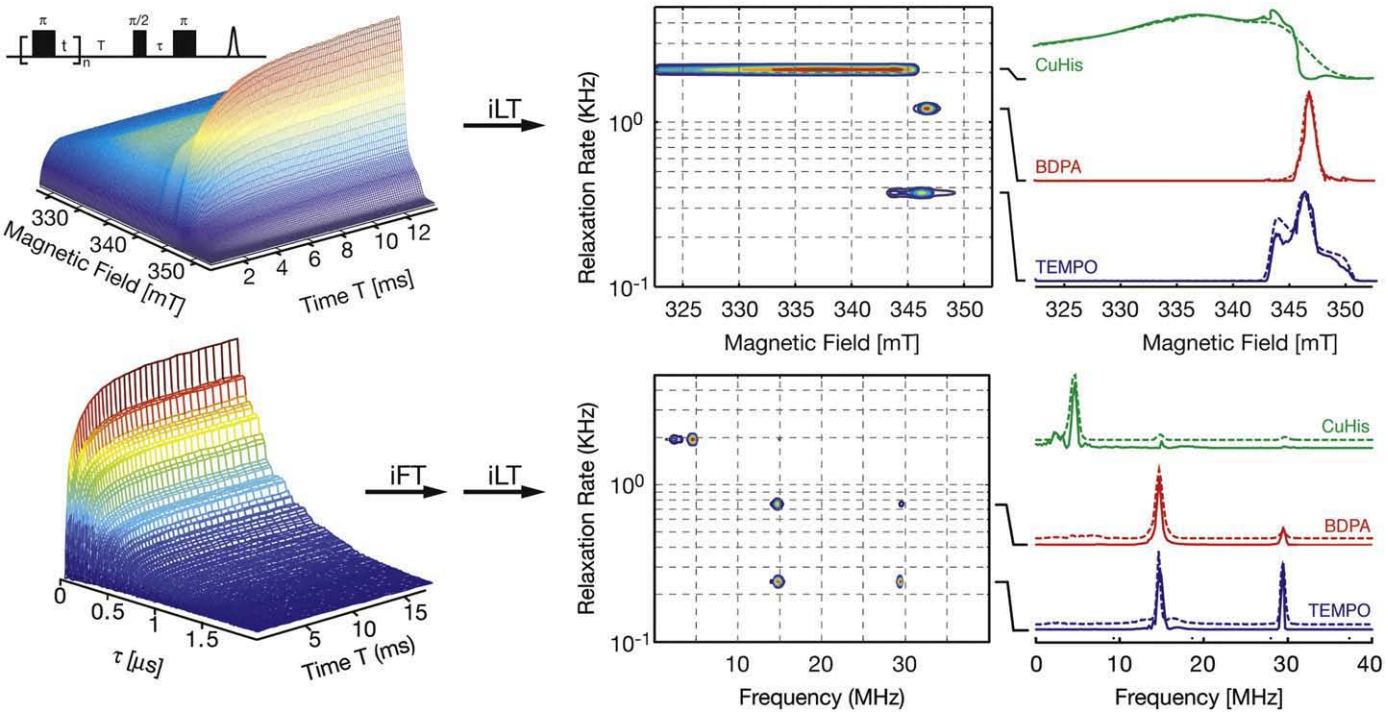

Fig. 10. (Top row) 9 GHz two-dimensional saturation-recovery field-sweep spectrum of a mixture of BDPA/PS, TEMPO/PS and CuHis (left). Inverse Laplace transformation of the data set yields the separated field-sweep spectra (right). The spectrum of the individual compound is compared with the spectra of the pure compound (dashed line). (Bottom row) 9 GHz two-dimensional REFINE-ESEEM spectrum of the same mixture (left). The separated ESEEM spectra are obtained by a Fourier transformation prior to the inverse Laplace transformation (right). The pulse sequence used for both experiments is shown in the top corner to the left. Both spectra are taken at $T = 20$ K. Figure adapted from [53].

identified by comparison with the spectra of the pure compounds. The fastest relaxing species is the Cu center of the CuHis complex (shown in green). The compound with the second fastest relaxation rate in the mixture is BDPA (shown in red), while the slowest relaxing species is TEMPO (shown in blue) under the given experimental conditions. In Fig. 10 (top, right), the individual traces, as obtained from the two-dimensional data set, are quantitatively compared with the echo-detected field-swept spectra of the pure compounds. In the high-field region, the separated CuHis spectrum is not reproduced very accurately, but the agreement is excellent for TEMPO and BDPA. Based on these results, a two-dimensional REFINE-ESEEM experiment was performed, to separate the overlapping hyperfine spectra of the three paramagnetic compounds. The experiment was conducted at a fixed field position of 346.3 mT. At this field position all three compounds overlap and contribute with similar amplitudes to the overall EPR signal. After inversion of the data, the relaxation encoded two-pulse ESEEM spectra are obtained in this dimension and three different hyperfine spectra can be distinguished (Fig. 10 bottom, left).

For both the BDPA and the TEMPO sample, transitions at around 14 and 28 MHz are observed. These are assigned to sq and dq ^{1}H transitions, indicating a proton electron hyperfine interaction as expected for these compounds. For the CuHis complex, which was crystallized from deuterated water, several ^{14}N and ^{2}H resonances were observed. Again, the three hyperfine spectra obtained by two-dimensional REFINE-ESEEM are quantitatively compared to hyperfine spectra recorded from the pure compounds (Fig. 10 bottom, right). All REFINE-ESEEM spectra show very good agreement with the hyperfine spectra of the pure compounds measured individually. In particular

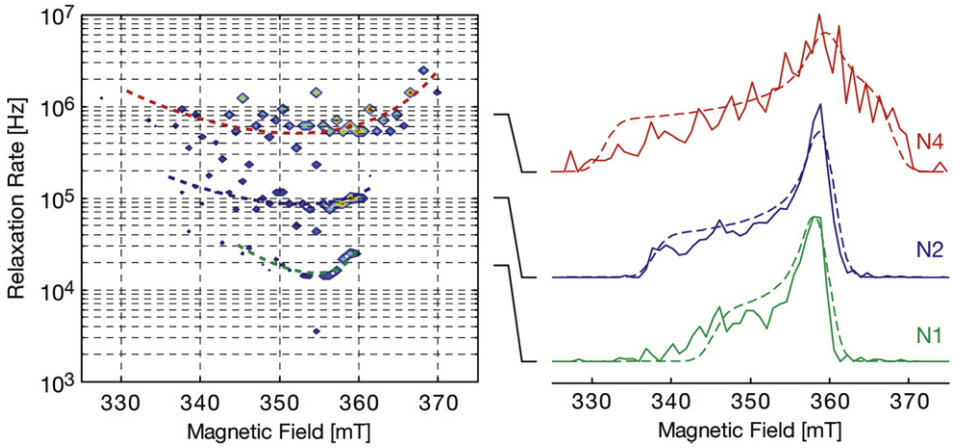

Fig. 11. Two-dimensional 9 GHz relaxation-filtered echo-detected field sweep spectra of complex I from *Y. lipolytica* taken at 12 K after inversion of the experimental data set. (Left side) Contour plot of the spectrum obtained after inversion. The ridges (dashed lines) are guides for the eyes. (Right side) Individual slices generated by following the ridges in the contour plot and projecting the intensity at an average value of the relaxation rate. Individual spectra (solid lines) are compared with the simulations of field-swept spectra (dashed lines) of cluster N1, N2 and N4 using the *g* values given in [62].

the amplitude ratios of the sq and dq peaks are conserved in the REFINE experiment and contributions of each species can clearly be distinguished by the different intensity ratio of sq to dq proton peaks. Also the weaker and much broader proton hyperfine coupling of methyl protons of TEMPO, which show up symmetrically around the free ^{1}H Larmor frequency can be detected in the REFINE spectra. As in the saturation-recovery detected field-sweep experiment, this comparison demonstrates that the separation of the hyperfine spectra of all three compounds is possible.

Preliminary results of two-dimensional REFINE applied to EPR spectra of complex I are shown in Fig. 11. The experiment was performed at a temperature of 12 K at which cluster N1, N2 and N4 contribute to the EPR signal. The relaxation domain was encoded using a picket-fence saturation sequence [53] and the inversion of experimental data set was achieved using the DISCRETE software package [59,60]. After inversion of the data set, three different species can be identified in the relaxation-encoded dimension. All three show a significant relaxation anisotropy as indicated by the dashed lines in Fig. 11 (right). After projecting the intensities of each species along the mean value of the respective filter rates, the EPR spectrum of cluster N1, N2 and N4 is obtained and compared with simulated EPR spectra of the individual FeS cluster and is in exactable agreement given the complexity of the system.

Currently the main limiting factor for the application of two-dimensional REFINE spectroscopy is the available algorithms for inversion of the experimental data set. However, in the future more sophisticated algorithms such as Tikhonov regularization will help to make this task more stable and therefore more widely applicable.

6. Summary and outlook

Pulsed EPR spectroscopy can help to understand the structure and function of complex biological systems that host paramagnetic centers, such as complex I of the mitochondrial respiratory chain. While a crystal structure gives a rather static picture of the architecture, EPR spectroscopy can give more detailed information about paramagnetic centers in their functional states. EPR reveals the identity of paramagnetic co-factors and gives detailed information of their ligand sphere. In recent years, more and more EPR techniques such as pulsed and high-field EPR became available, strongly improving the use of hyperfine and dipolar spectroscopy for biological applications. Here, we showed that REFINE can separate individual spectral contributions of different paramagnetic species based on their relaxation behavior, which allows assignment of hyperfine and dipolar couplings to the individual paramagnetic centers, for example, FeS clusters in electron transfer chains. Such a determination of the local ligand sphere and of the distances to the other paramagnetic centers in a protein will be a viable tool for their assignment in X-ray structures. For complex I of the mitochondrial respiratory chain, such work is currently in progress.

Acknowledgements

The authors thank Fraser MacMillan (University of East Anglia, Norwich, UK) for helpful discussions. This work was supported by the Sonderforschungsbereich SFB 472 “Molecular Bioenergetics”, projects P2, P15 and the Center for Biomolecular Magnetic Resonance (BMRZ) Frankfurt. A. C. is grateful for a stipend of the International Max-Planck Research School for Membrane Proteins.

References

[1] J. Stubbe, W.A. van der Donk, Protein radicals in enzyme catalysis, Chem. Rev. 98 (1998) 705–762.
[2] T. Prisner, M. Rohrer, F. MacMillan, Pulsed EPR spectroscopy: biological applications, Annu. Rev. Phys. Chem. 52 (2001) 279–313.
[3] M. Bennati, T.F. Prisner, New developments in high field Electron Paramagnetic Resonance with applications in structural biology, Rep. Prog. Phys. 68 (2005) 411–448.
[4] W. Lubitz, E. Reijerse, M. van Gastel, [NiFe] and [FeFe] hydrogenases studied by advanced magnetic resonance techniques, Chem. Rev. 107 (2007) 4331–4365.
[5] G. Jeschke, Y. Polyhach, Distance measurements on spin-labelled biomacromolecules by pulsed Electron Paramagnetic Resonance. Phys. Chem. Chem. Phys. 9 (2007) 1895–1910.
[6] B.E. Bode, J. Plackmeyer, T.F. Prisner, O. Schiemann, PELDOR measurements on a nitroxide-labeled Cu(II) porphyrin: orientation selection, spin-density distribution, and conformational flexibility, J. Phys. Chem. A 112 (2008) 5064–5073.
[7] B.M. Hoffman, ENDOR of metalloenzymes, Acc. Chem. Res. 36 (2003) 522–529.
[8] M. Hertel, V. Denysenkov, M. Bennati, T. Prisner, Pulsed 180-GHz EPR/ENDOR/PELDOR spectroscopy. Magn. Reson. Chem. 43 (2005) S248–255.
[9] H. Blok, J.A.J.M. Disselhorst, H. van der Meer, S.B. Orlinskii, J. Schmidt, ENDOR spectroscopy at 275 GHz, J. Magn. Reson. 173 (2005) 49–53.
[10] A. Schweiger, G. Jeschke, Principles of Pulse Electron Paramagnetic Resonance, Oxford University Press, Oxford, UK, 2001.
[11] S.S. Eaton, G.R. Eaton, Relaxation time of organic radicals and transition metals, in: L.J. Berliner, S.S. Eaton, G.R. Eaton (Eds.), Biological Magnetic Resonance: Distance Measurements in Biological Systems by EPR, vol. 19, 2000.
[12] C. Lawrence, M. Bennati, H. Obias, G. Bar, R. Griffin, J. Stubbe, High-field EPR detection of a disulfide radical anion in the reduction of cytidine 5′-diphosphate by the E441Q R1 mutant of *Escherichia coli* ribonucleotide reductase. Proc. Nat. Aca. Sci. U. S. A. 96 (1999) 8979–8984.
[13] H. Yoshida, T. Ichikawa, Electron spin echo studies of free radicals in irradiated polymers, Rec. Trends Rad. Pol. Chem. (1993) 3–36.
[14] A. Videira, Complex I from the fungus *Neurospora crassa*, Biochim. Biophys. Act. 1364 (1998) 89–100.
[15] U. Brandt, S. Kerscher, S. Droese, K. Zwicker, V. Zickermann, Proton pumping by NADH:ubiquinone oxidoreductase. A redox driven conformational change mechanism? FEBS Lett. 545 (2003) 9–17.
[16] M. Wikstroem, Two protons are pumped from the mitochondrial matrix per electron transferred between NADH and ubiquinone, FEBS Lett. 169 (1984) 300–304.
[17] H. Weiss, T. Friedrich, Redox-linked proton translocation by NADH–ubiquinone reductase (complex I), J. Bioen. Biomem. 23 (1991) 743–754.
[18] A.H.V. Schapira, Human complex I defects in neurodegenerative diseases, Biochim. Biophys. Act. 1364 (1998) 261–270.
[19] B.H. Robinson, Human complex I deficiency: clinical spectrum and involvement of oxygen free radicals in the pathogenicity of the defect, Biochim. Biophys. Act. 1364 (1998) 271–286.
[20] R.S. Balaban, S. Nemoto, T. Finkel, Mitochondria, oxidants, and aging, Cell 120 (2005) 483–495.
[21] J. Hirst, J. Carroll, I. Fearnley, R. Shannon, J. Walker, The nuclear encoded subunits of complex I from bovine heart mitochondria. Biochim. Biophys. Act. 1604 (2003) 135–150.
[22] T. Yagi, T. Yano, S. Di Bernardo, A. Matsuno-Yagi, Procaryotic complex I (NDH-1), an overview. Biochim. Biophys. Acta 1364 (1998) 125–133.
[23] S. Kerscher, S. Droese, K. Zwicker, V. Zickermann, U. Brandt, *Yarrowia lipolytica*, a yeast genetic system to study mitochondrial complex I, Biochim. Biophys. Acta 1555 (2002) 83–91.
[24] D.-C. Wang, S.W. Meinhardt, U. Sackmann, H. Weiss, T. Ohnishi, The iron–sulfur clusters in the two related forms of mitochondrial NADH: ubiquinone oxidoreductase made by *Neurospora crassa*, Eur. J. Biochem. 197 (1991) 257–264.
[25] N. Morgner, V. Zickermann, S. Kerscher, I. Wittig, A. Abdrakhmanova, H.-D. Barth, B. Brutschy, U. Brandt, Subunit mass fingerprinting of mitochondrial complex I, Biochim. Biophys. Acta 1777 (2008) 1384–1391.
[26] N. Grigorieff, Three-dimensional structure of bovine NADH:ubiquinone oxidoreductase (complex I) at 22 Å in ice, J. Mol. Bio. 277 (1998) 1033–1046.
[27] V. Guénebaut, A. Schlitt, H. Weiss, K. Leonard, T. Friedrich, Consistent structure between bacterial and mitochondrial NADH:ubiquinone oxidoreductase (complex I), J. Mol. Bio. 276 (1998) 105–112.
[28] G. Peng, G. Fritzsch, V. Zickermann, H. Schagger, R. Mentele, F. Lottspeich, M. Bostina, M. Radermacher, R. Huber, K.O. Stetter, H. Michel, Isolation, characterization and electron microscopic single particle analysis of the NADH:ubiquinone oxidoreductase (Complex I) from the hyperthermophilic eubacterium *Aquifex aeolicus*, Biochemistry 42 (2003) 3032–3039.
[29] M. Radermacher, T. Ruiz, T. Clason, S. Benjamin, U. Brandt, V. Zickermann, The three-dimensional structure of complex I from *Yarrowia lipolytica*: a highly dynamic enzyme, J. Struct. Biol. 154 (2006) 269–279.
[30] T. Ohnishi, Iron–sulfur clusters/semiquinones in complex I. Biochim. Biophys. Act. 1364 (1998) 186–206.
[31] T. Ohnishi, E. Nakamaru-Ogiso, Were there any “misassignments” among iron–sulfur clusters N4, N5 and N6b in NADH–quinone oxidoreductase (complex I)? Biochim. Biophys. Act. 1777 (2008) 703–710.
[32] G. Yakovlev, T. Reda, J. Hirst, Reevaluating the relationship between EPR spectra and enzyme structure for the iron–sulfur clusters in NADH:quinone oxidoreductase, Proc. Nat. Aca. Sci. USA 104 (2007) 12720–12725.
[33] T. Yano, T. Ohnishi, The origin of cluster N2 of the energy-transducing NADH–quinone oxidoreductase: comparisons of phylogenetically related enzymes, J. Bioen. Biomem. 33 (2001) 213–222.
[34] R. van Belzen, A.B. Kotlyar, N. Moon, W.R. Dunham, S.P.J. Albracht, The iron–sulfur clusters 2 and ubisemiquinone radicals of NADH:ubiquinone oxidoreductase are involved in energy coupling in submitochondrial particles, Biochemistry 36 (1997) 886–893.
[35] P. Hinchliffe, L. Sazanov, Organization of iron–sulfur clusters in respiratory complex I. Science 309 (2005) 771–774.

[36] L. Sazanov, P. Hinchliffe, Structure of the hydrophilic domain of respiratory complex I from *Thermus thermophilus*, Science 311 (2006) 1430–14306.
[37] G.H. Rist, J.S. Hyde, Ligand ENDOR of metal complexes in powders, J. Chem. Phys. 52 (1970) 4633–4643.
[38] R.D. Britt, K. Sauer, M.P. Klein, D.B. Knaff, A. Kriauciunas, C.A. Yu, L. Yu, R. Malkin, Electron Spin Echo Envelope Modulation spectroscopy supports the suggested coordination of two histidine ligands to the Rieske iron–sulfur centers of the cytochrome b6f complex on spinach and the cytochrome bc1 complexes of *Rhodospirillum rubrum*, *Rhodobacter sphaeroides* R-26, and bovine heart mitochondria, Biochemistry 30 (1991) 1892–1901.
[39] R. Cammack, A. Chapman, J. McCracken, J.B. Cornelius, J. Peisach, J.H. Weiner, Electron spin-echo spectroscopic studies of *Escherichia coli* fumarate reductase, Biochim. Biophys. Act. 956 (1988) 307–312.
[40] S.A. Dikanov, A.M. Tyryshkin, I. Felli, E.J. Reijerse, J. Huttermann, C-band ESEEM of strongly coupled peptide nitrogens in reduced two-iron ferredoxin, J. Magn. Reson. Ser. B 108 (1995) 99–102.
[41] T. Maly, L. Grgic, K. Zwicker, V. Zickermann, U. Brandt, T. Prisner, Cluster N1 of complex I from *Yarrowia lipolytica* studied by pulsed EPR spectroscopy. J. Biol. Inorg. Chem. 11 (2006) 343–350.
[42] L. Kevan, M.K. Bowman, Modern Pulsed and Continuous-wave Electron Spin Resonance, Wiley, New York, 1990.
[43] S. Dikanov, A. Tyryshkin, M. Bowman, Intensity of cross-peaks in HYSCORE spectra of $S=1/2$, $I=1/2$ spin systems. J. Magn. Reson. 144 (2000) 228–242.
[44] S. Van Doorslaer, A. Schweiger, A two-dimensional sum combination frequency pulse EPR experiment, Chem. Phys. Lett. 281 (1997) 297–305.
[45] C. Canne, M. Ebelshauser, E. Gay, J.K. Shergill, R. Cammack, R. Kappl, J. Huttermann, Probing magnetic properties of the reduced [2Fe–2S] cluster of the ferredoxin from *Arthrospira platensis* by 1H ENDOR spectroscopy, J. Biol. Inorg. Chem. 5 (2000) 514–526.
[46] R. Kappl, S. Ciurli, C. Luchinat, J. Huttermann, Probing structural and electronic properties of the oxidized [Fe4S4]3+ cluster of *Ectothiorhodospira halophila* iso-II high-potential iron–sulfur protein by ENDOR spectroscopy, J. Am. Chem. Soc. 121 (1999) 1925–1935.
[47] C. Gemperle, G. Aebli, A. Schweiger, R.R. Ernst, Phase cycling in pulse EPR, J. Magn. Reson. 88 (1990) 241–256.
[48] A. Garofano, K. Zwicker, S. Kerscher, P. Okun, U. Brandt, Two aspartic acid residues in the PSST-homologous NUKM subunit of complex I from *Yarrowia lipolytica* are essential for catalytic activity, J. Biol. Chem. 278 (2003) 42435–42440.
[49] N. Kashani-Poor, S. Kerscher, V. Zickermann, U. Brandt, Efficient large scale purification of his-tagged proton translocating NADH:ubiquinone oxidoreductase (complex I) from the strictly aerobic yeast *Yarrowia lipolytica*, Biochim. Biophys. Act. 1504 (2001) 363–370.
[50] T. Maly, F. MacMillan, K. Zwicker, N. Kashani-Poor, U. Brandt, T. Prisner, Relaxation Filtered Hyperfine (REFINE) spectroscopy: a novel tool for studying overlapping biological Electron Paramagnetic Resonance signals applied to mitochondrial complex I. Biochemistry 43 (2004) 3969–3978.
[51] J. Harmer, C. Finazzo, R. Piskorski, S. Ebner, E.C. Duin, M. Goenrich, R.K. Thauer, M. Reiher, A. Schweiger, D. Hinderberger, B. Jaun, A nickel hydride complex in the active site of methyl-coenzyme M reductase: implications for the catalytic cycle, J. Am. Chem. Soc. 130 (2008) 10907–10920.
[52] H. Dube, B. Kasumaj, C. Calle, M. Saito, G. Jeschke, F. Diederich, Direct evidence for a hydrogen bond to bound dioxygen in a myoglobin/hemoglobin model system and in cobalt myoglobin by pulse-EPR spectroscopy, Angew. Chem. Int. Ed. 47 (2008) 2600–2603.
[53] A. Cernescu, T. Maly, T.F. Prisner, 2D-REFINE spectroscopy: separation of overlapping hyperfine spectra, J. Magn. Reson. 192 (2008) 78–84.
[54] I.J.D. Craig, A.M. Thompson, Why Laplace transforms are difficult to invert numerically, Comp. Phys. 8 (1994) 648–654.
[55] C.S. Johnson, Diffusion ordered Nuclear Magnetic Resonance spectroscopy: principles and applications, Prog. NMR. Spec. 34 (1999) 203–256.
[56] A. Lupulescu, M. Kotecha, L. Frydman, Relaxation-assisted separation of chemical sites in NMR spectroscopy of static solids, J. Am. Chem. Soc. 125 (2003) 3376–3383.
[57] J. Kauppinen, J. Partanen, Fourier Transforms in Spectroscopy, 1st ed.Wiley-VCH, Berlin ; New York, 2001.
[58] M. Rohrer, P. Gast, K. Mobius, T.F. Prisner, Anisotropic motion of semiquinones in photosynthetic reaction centers of *Rhodobacter sphaeroides* R26 and in frozen isopropanol solution as measured by pulsed high-field EPR at 95 GHz, Chem. Phys. Lett. 259 (1996) 523–530.
[59] S.W. Provencher, An eigenfunction expansion method for the analysis of exponential decay curves, J. Chem. Phys. 64 (1976) 2772–2777.
[60] S.W. Provencher, R.H. Vogel, Information loss with transform methods in system identification: a new set of transforms with high information content, Math. Biosci. 50 (1980) 251–262.
[61] T. Maly, T. Prisner, Relaxation Filtered Hyperfine spectroscopy (REFINE), J. Magn. Reson. 170 (2004) 88–96.
[62] R. Djafarzadeh, S. Kerscher, K. Zwicker, M. Radermacher, M. Lindahl, H. Schagger, U. Brandt, Biophysical and structural characterization of proton-translocating NADH-dehydrogenase (complex I) from the strictly aerobic yeast *Yarrowia lipolytica*. Biochim. Biophys. Act. 1459 (2000) 230–238.